

POST MISSION DISPOSAL CONSIDERATIONS FOR ROCKET STAGES

Lucía Ayala Fernández⁽¹⁾, Carsten Wiedemann⁽²⁾, Simona Silvestri⁽²⁾, Vitali Braun⁽³⁾, and Stijn Lemmens⁽⁴⁾

⁽¹⁾*Technische Universität Braunschweig, now at Terma Group 64293 Darmstadt, Germany, Email: lafe@terma.com*

⁽²⁾*Technische Universität Braunschweig, 38108 Braunschweig, Germany*

⁽³⁾*IMS Space Consultancy GmbH at ESA/ESOC, 64293 Darmstadt, Germany*

⁽⁴⁾*European Space Agency, ESTEC, 2201 Noordwijk, Netherlands*

ABSTRACT

The Post-Mission Disposal (PMD) of rocket stages is a crucial aspect in the efforts towards the sustainability of space operations. This paper gives an overview of the main results of the ASCenSIon (Advancing Space Access Capabilities - Reusability and Multiple Satellite Injection) project on different aspects related to the PMD of rocket stages. The aim was to get a better understanding of current PMD practices and of the uncertainties present in current methods to assess the orbital lifetime, and investigate methodologies to improve these predictions.

The results provide an insight of different factors that affect the accuracy of orbital lifetime predictions in Low Earth Orbit (LEO). Moreover, it was shown that the estimation of the ballistic coefficient of rocket stages on-orbit from their Two-Line Elements (TLEs) can help to improve orbital lifetime predictions of future similar stages. Finally, the PMD practices of different launcher families were analyzed in regard to their compliance with current space debris mitigation guidelines.

Keywords: Rocket body, Post-Mission Disposal, orbital lifetime, ballistic coefficient.

1. INTRODUCTION

This paper aims to summarize some of the results of the ASCenSIon project related to the Post-Mission Disposal (PMD) of rocket stages. Some of these results have already been presented by the authors in past conferences and journal papers [14, 13, 12]. The current work provides a general picture of the analyses performed, as well as additional insights, which are detailed in each section.

The PMD of spacecraft and rocket stages, once their mission has concluded, is an essential aspect of space debris mitigation measures. It aims at reducing the risk of further creation of space debris caused by on-orbit explosions or collisions. An integral part of PMD is the clearance from the protected regions, as stated in the IADC (Inter-Agency Space Debris Coordination Committee)

space debris mitigation guidelines [8]. More specifically, these guidelines establish that objects crossing the Low Earth Orbit (LEO) region should re-enter into Earth's atmosphere within a maximum of 25 years after the end of their mission. Moreover, the Zero Debris policy reduces this limit to 5 years orbital lifetime after the end of the mission and adds one further requirement: the cumulative collision probability (CCP) of an object with respect to the 1cm population, from the end of its mission until its re-entry, should not exceed 1 in 1000 [10].

The analyses presented in this paper aim to analyze the compliance with these requirements by current rocket stages, to gain a better understanding of the uncertainties to be considered when assessing this compliance, and to investigate methodologies to improve such assessments.

The scope of these analyses focuses on the study of rocket stages, which will be called rocket bodies (RBs) throughout this paper. RBs are a very distinct type of space objects for several reasons: firstly, their mission typically ends very shortly after reaching orbit. Moreover, they tend to have a cylindrical shape (often with a "cone" attached). These shared characteristics make the RBs a suitable target group for this study. Additionally, many of the heaviest objects among the space debris population are RBs, and they are also the main source of on-orbit fragmentations [15]. This highlights the importance of assessing space debris mitigation practices for RBs.

Furthermore, the focus is on objects that cross the LEO region, which is defined by a 2000 km limit in altitude. Two different orbital regimes will be distinguished: orbits which are contained in the LEO region, thus the apogee altitude is below 2000 km; and Highly-Eccentric Orbits (HEO), which in this work are defined as orbits with a perigee altitude below 2000 km and apogee altitude above 2000 km. For simplicity, objects in each of these orbital regimes will be called LEO objects and HEO objects respectively.

The driving perturbation leading to the re-entry of objects in the LEO region is the drag force. Due to the large eccentricity of HEO orbits, other forces become also relevant, such as gravitational third-body perturbations coming from the Moon and the Sun, and solar radiation pres-

sure. These complex dynamics represent a big challenge for the estimation of the orbital lifetime of objects in these orbits, as they are very sensible to changes in the initial conditions [19, 21].

The physical characteristics of an object that determine its susceptibility to drag can be consolidated into a single parameter known as the ballistic coefficient $B = m/(A \cdot c_D)$, where A is the cross-section of the object that faces drag, thus in the direction of the velocity, c_D is the drag coefficient and m is the mass of the object. This parameter will be extensively studied in this paper, as well as different ways of estimating the future solar and geomagnetic activity, due to their high impact on orbital lifetime estimations.

For the studies in this paper, the tool OSCAR (Orbital SpaceCraft Active Removal) from the DRAMA 3.1.0 (Debris Risk Assessment and Mitigation Analysis) software suite was used, which is the standard tool of the European Space Agency to assess PMD strategies and is freely available online¹. OSCAR allows to assess the remaining orbital lifetime of an object considering different solar and geomagnetic activity scenarios. It uses a semi-analytical propagator, FOCUS (Fast Orbit Computation Utility Software), which takes singly averaged orbital elements and uses a variable-step multi-step predictor/corrector integrator. In the version used in OSCAR, FOCUS considers geopotential terms up to the 6th order, atmospheric drag using the thermosphere model NRLMSISE-00, third body perturbations caused by the gravitational forces of the Moon and the Sun, and solar radiation pressure (SRP) considering a cylindrical Earth shadow.

This paper is structured in the following way: first, the accuracy of orbital lifetime predictions with OSCAR for rocket bodies is analyzed, using the recommended solar and geomagnetic activity scenarios and testing two different hypotheses for the drag coefficient c_D . Subsequently, the tool RACER (Radiation and Atmospheric Drag Coefficient Estimation Routine) is used to estimate the ballistic coefficient of a group of stages, and the results are used to improve the orbital lifetime predictions of similar stages. Finally, an analysis of the PMD practices of the main rocket families is presented, including their orbital lifetimes and CCP with respect to the 1 cm population, in accordance to the Zero Debris policy.

2. ACCURACY OF LIFETIME PREDICTIONS

This analysis aims to investigate the accuracy of current methods used for orbital lifetime predictions applied to rocket stages. To do so, the initial orbits of 770 rocket bodies were propagated using OSCAR. The rocket bodies chosen for the study have already re-entered, which provided an objective reality to compare with. The propagations were performed using different solar and geo-

magnetic activity scenarios as well as different assumptions for the estimation of the drag coefficient, as both are parameters that can greatly influence orbital lifetime predictions. The content of this section was presented in detail in [14]. The current paper adds the latest prediction scenario for the solar and geomagnetic activity, and an analysis of the impact of the ballistic coefficient on the accuracy of the predictions in LEO and of the Sun-synchronous resonance on the predictions in HEO.

2.1. Dataset and Methodology

The dataset used was extracted from the DISCOS (Database and Information System Characterising Objects in Space) database. In order to select the objects relevant for the study, the following characteristics had to be met:

1. Object type is Rocket Body (RB).
2. The perigee of the object is below 2,000 km altitude.
3. The object has already re-entered.
4. The object had been orbiting Earth for at least 1 year.
5. The object has information about its mass, cross-section, and initial orbit registered in DISCOS.
6. The object did not undergo a fragmentation.
7. At least 10 Two Line Elements (TLEs) of the object are available.

These requirements resulted in a dataset of 770 objects, which were separated in 340 LEO objects and 430 HEO objects.

The initial orbits of the objects of the dataset were propagated with OSCAR until their re-entry in order to compare the estimated orbital lifetime with the actual orbital lifetime of the objects. For the LEO objects, the initial orbits registered in DISCOS were used for the propagation. These registered initial orbits include the semimajor axis, the eccentricity, and the inclination of the orbit, as well as the argument of periapsis for some of them. However, the right ascension of the ascending node (RAAN) is typically not included. This is an important parameter for HEO orbits, which are highly influenced by third-body perturbations originated by the Sun and the Moon (also called lunisolar perturbations). Therefore, the first TLE of each of the HEO objects was used as the initial orbit for the propagation. The TLEs used in this study were extracted from [4]. It is also important to note that TLEs include doubly-averaged orbital elements, while OSCAR takes singly averaged ones. The appropriate conversions were performed with the CState tool, also available in DRAMA.

¹<https://sdup.esoc.esa.int/>

Also important for the propagation are the physical properties of the propagated objects. In this case, the mass and the average cross-section of the rocket bodies registered in DISCOS were used for the propagation. Furthermore, two different cases were used for the drag coefficient, c_D , of the objects:

1. Using a default $c_D = 2.2$ for all the rocket bodies. This is a very common assumption, as well as the default in OSCAR.
2. Considering that rocket bodies can be approximated as cylinders. The drag coefficient of a randomly tumbling cylinder in a free molecular flow can be calculated as [18]:

$$c_D = 1.57 + 0.785 \cdot \frac{D}{L} \quad (1)$$

Where D is the diameter and L is the length of the cylinder. In this case, the c_D of each rocket body was estimated individually, using the dimensions available on DISCOS.

When the predicted lifetime of an object differed very strongly from the observed one, both the initial orbit and physical characteristics of the stage were checked in order to detect and correct errors in the database or in the TLE used that could be affecting the propagation. This process reduced significantly the number of outliers in the results. However, it is important to note that the results are still susceptible to underlying errors in the data.

An important factor when the orbit of an object is propagated into the future is the solar and geomagnetic activity considered. Both parameters are important inputs in atmospheric models, strongly influencing the atmospheric density and, therefore, the drag that is experienced by an object. Four different scenarios were chosen for this analysis. Three of them are recommended in [7, 17], while the fourth one simply makes use of the recorded solar and geomagnetic activity taking advantage of the fact that the propagations in this analysis take place in the past:

1. Reference: uses the observed solar and geomagnetic activity. This is not possible when missions are planned into the future but allows us to identify the uncertainties in the model that remain even when the solar and geomagnetic activity is known. This was done in OSCAR by simply running the propagations with the latest prediction scenario, as it takes the known activity when there is one.
2. Monte Carlo: the solar and geomagnetic activity used corresponds to an equivalent day of the cycle within one of the preceding five solar cycles, which is randomly selected [16].
3. ECSS cycle: this approach consists of repeating the 23rd solar cycle as many times as appropriate for the propagation span, considering the position within the solar cycle at the start of the propagation [16].
4. Latest prediction or best guess: the future behavior is estimated based on the current sunspot cycle and based on sampled past cycles [16]. To achieve this behavior, the solar activity files were modified for each propagation so that only the solar and geomagnetic activity before the launch date was known.

The outcome of the propagation with OSCAR is a trajectory until re-entry for each object, which leads to a predicted re-entry epoch and an estimated orbital lifetime. The error in the prediction of the orbital lifetime, is defined as the difference between the predicted re-entry epoch and the observed one. Thus, a negative error will indicate an underestimation of the orbital lifetime, while a positive error indicates an overestimation of the orbital lifetime. Moreover, the relative error was defined by normalizing the resulting error with the observed orbital lifetime of the objects.

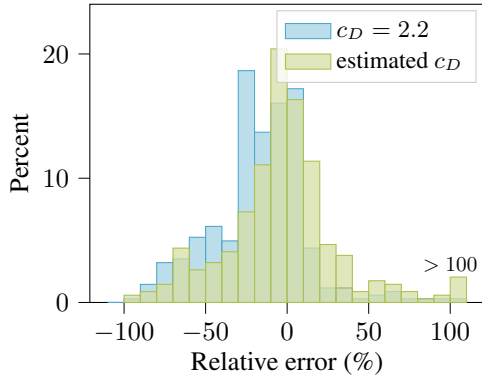
2.2. Results in LEO

The histograms in figure 1 show the comparison of the relative error distribution for the two c_D for all the solar and geomagnetic activity scenarios. The results with the default $c_D = 2.2$ show a skewness towards negative values for the first three scenarios, which shows a tendency to underestimate the orbital lifetime confirmed by average errors of around -15%. The average error for the latest prediction scenario was on the positive range, with $\approx 8\%$, but this is highly influenced by some strong outliers. The median, on the other hand, remained negative, and the standard deviation was close to a 60% while for the other three scenarios, it remained around 30%.

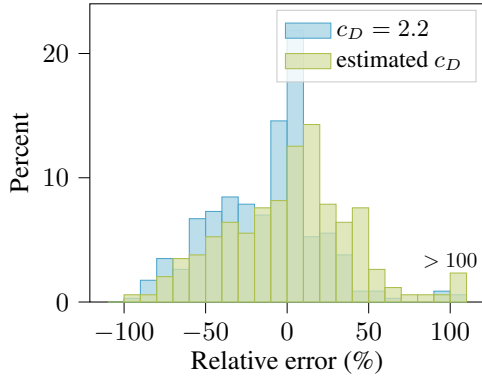
The use of the estimated c_D caused significant changes in the distributions. In the reference scenario, it seems to "correct" the skewness of the distribution, leading to a seemingly "normal" distribution centered closely around 0. The distribution of the error for the Monte Carlo and ECSS cycle scenarios also shifted towards more positive values, which also led to mean values closer to zero while keeping a similar standard deviation. However, there is no clear improvement in the results for the latest prediction scenario.

As the results in the reference scenario showed a clear improvement, correcting the tendency to underestimate the orbital lifetime, it can be concluded that the assumptions made to estimate the drag coefficient with equation (1) seem valid, or lead to more accurate results than the default 2.2, for the RBs in the studied dataset. This conclusion is based on the fact that the reference scenario uses the observed solar and geomagnetic activity, while other scenarios are affected by the errors in the predictions of the solar cycle.

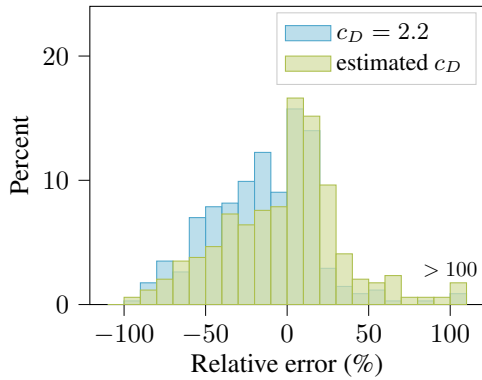
There are, however, many parameters that influence the accuracy of orbital lifetime predictions. For instance, the launch year has a strong effect as it influences how accurate the solar and geomagnetic scenarios used were in



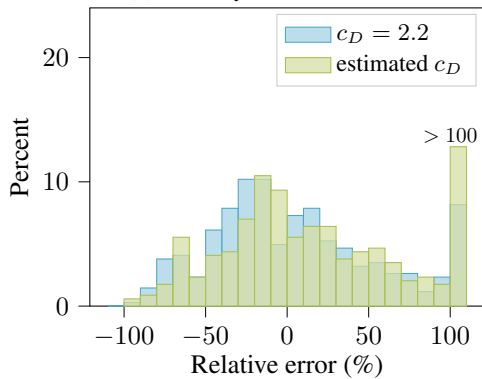
(a) Reference scenario.



(b) Monte Carlo scenario.



(c) ECSS cycle scenario.



(d) Latest prediction scenario.

Figure 1: Comparison of the distribution of the relative error for the two cases for the c_D for each solar and geomagnetic activity scenario.

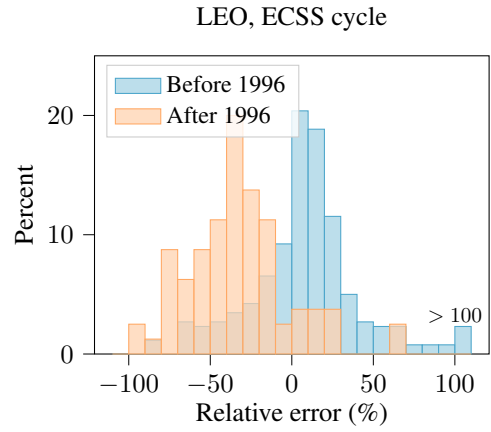


Figure 2: Distribution of the relative error for ECSS cycle scenario, using the estimated c_D , of objects launched before and after the 1st of August 1996.

comparison to the actual ones. An example of this effect is shown in figure 2, where the distribution of the error on the orbital lifetime predictions of objects launched before August 1996 is compared to objects launched afterwards, using the ECSS cycle scenario for the predictions. This date was chosen because it marks the start of the solar cycle number 23, which is the one used on the ECSS cycle scenario. Two very distinct distributions can be observed, where the objects launched after the start of cycle 23 suffer a strong underestimation of their orbital lifetimes, while the objects launched before present a slight overestimation. This is due to the fact that the solar cycles before cycle 23 were on average more active, leading to higher atmospheric density and a faster orbital decay, while cycle 24 was significantly weaker than cycle 23, leading to longer orbital lifetimes than expected.

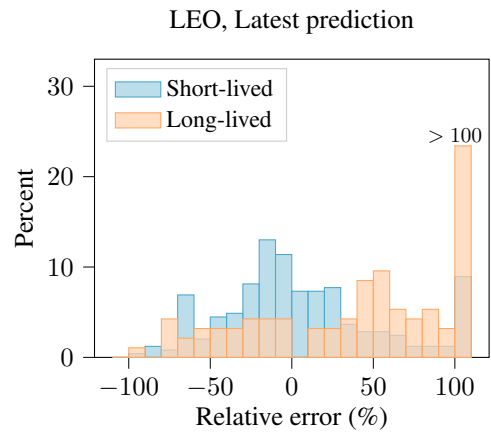


Figure 3: Comparison of the distribution of the relative error for long and short-lived objects in LEO, using the estimated c_D and for the latest prediction scenario.

Another aspect influencing the accuracy of the predictions is how long the objects actually stayed on orbit. Figure 3 shows the distribution of the error for long- and short-lived objects using the latest prediction solar and

geomagnetic activity scenario. Long-lived objects were defined as those which were on orbit for more than 10 years, while short-lived objects re-entered faster than 10 years. The distribution of the long-lived objects appears to be more spread, almost random, and with a very high proportion of objects with errors above 100%. This effect was originated in the underestimation of the solar and geomagnetic activity for several solar cycles, leading to a build-up in the error.

Moreover, the ballistic coefficient B of the objects being analyzed also has an impact on the accuracy of the predictions, as it determines how affected the objects are by drag, and therefore also how affected they are by these uncertainties. Figure 4 shows the distribution of the error for objects with a ballistic coefficient below 50 kg/m^2 or above. The objects with a low B present a more spread distribution, as they are more sensible to small errors on the predictions of the solar cycle, errors on the atmospheric model, etc.

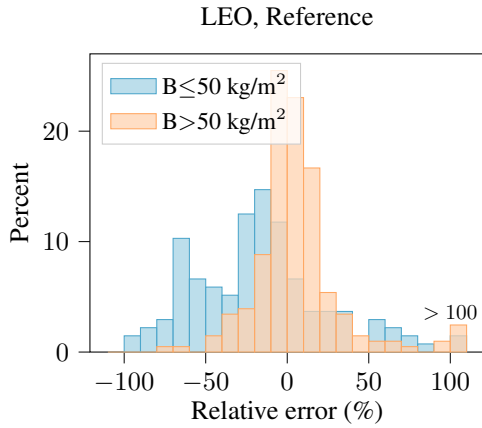


Figure 4: Comparison of the distribution of the relative error for objects with high and low ballistic coefficient in LEO, using the estimated c_D and for the reference solar and geomagnetic activity scenario.

It can be noticed that there are many nuances in the effects of these factors, that also change for the different solar and geomagnetic activity scenarios. It is therefore recommended to read [14] for a more complete picture.

2.3. Results in HEO

Figure 5 shows the results obtained for the objects in HEO, comparing the two c_D cases for each solar and geomagnetic activity scenario. The distribution of the error for these objects is significantly more spread than for the objects in LEO, featuring also a notably high number of outliers. This resulted in huge standard deviations, which were well above 100% for all the scenarios. Moreover, the distribution of the error appears to be very similar for all solar and geomagnetic activity scenarios. This is due to the smaller effect of the atmospheric drag on HEO objects, and therefore smaller differences between scenarios. For the same reason, the use of the estimated c_D

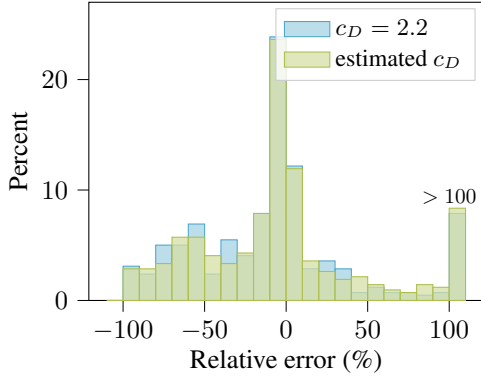
did not provoke any important changes in the distribution compared to the default c_D .

These results were not unexpected for HEO, and are caused by the high sensitivity of these orbits to initial conditions. One main reason for this sensitivity is the so called Sun-synchronous resonance, originated by the coupling between the drag force and third-body gravity attraction from the Sun.

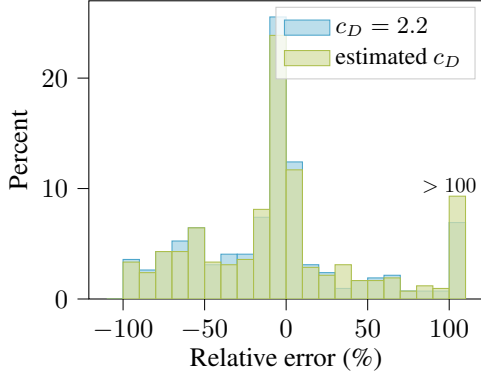
The orientation of the orbit with respect to the Sun, described by the Sun angle α , determines how the third-body gravity attraction from the Sun modifies the orbit. More specifically, the altitude of the perigee will increase when $0^\circ < \alpha < 90^\circ$ or $180^\circ < \alpha < 270^\circ$, and it will decrease when $90^\circ < \alpha < 180^\circ$ or $270^\circ < \alpha < 360^\circ$. During the natural evolution of HEO orbits, as the drag makes the semimajor axis decrease, Sun-synchronous or near Sun-synchronous conditions can be reached. When this happens, the Sun angle remains nearly constant for a long time. If Sun-synchronous conditions are reached when α is such that the altitude of perigee decreases, the re-entry is simply accelerated. However, if Sun-synchronous conditions are reached when α is such that the perigee altitude increases, the perigee can be raised to altitudes where the drag has almost negligible impact, drastically increasing the orbital lifetime. Moreover, as Sun-synchronous conditions are a result of the specific combination of eccentricity, inclination and semimajor axis, the rise of the perigee also delays the evolution of the semimajor axis so that the Sun-synchronous conditions will be maintained for a longer period of time, which in turn means that the perigee will keep rising for longer.

The Sun-synchronous resonance represents one of the biggest challenges in the prediction of orbital lifetime of objects in HEO orbits, due to the complex nature of this coupling between the drag force and the third-body gravity attraction from the Sun, the high sensitivity to entry conditions on the resonance, and the intrinsic challenges of drag modelling, which include the prediction of the solar cycle and the modelling of the atmosphere. However, not all HEO orbits are bound to reach the Sun-synchronous resonance. As it is possible to determine whether Sun-synchronous conditions are met from their orbital parameters, it is possible to divide the HEO objects into those that reach Sun-synchronous conditions at some point of their orbital evolution and those which do not. The results obtained for the reference scenario are shown in figure 6, with very similar results obtained for all the other scenarios as well.

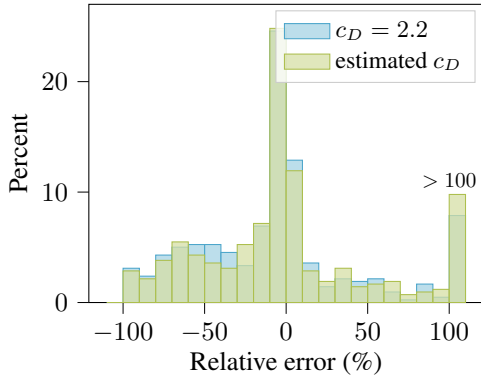
The results show a remarkable difference on the distribution of the error between the HEO objects that reach resonance conditions and those which do not. Those which reach resonant conditions show a distribution of the error that is rather random with a standard deviation above 150%, meaning that there is little to no confidence on the orbital lifetime predictions. However, the objects that do not reach the Sun-synchronous resonance show a clear distribution centered around zero, with a strong peak and



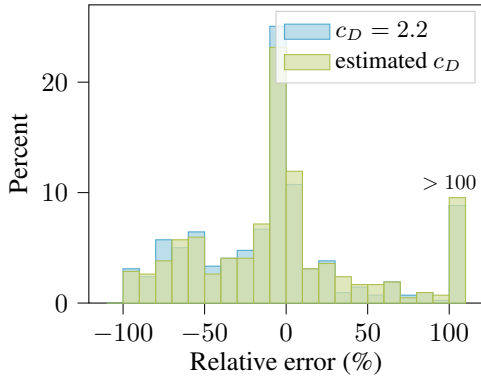
(a) reference scenario.



(b) Monte Carlo scenario.



(c) Repeated cycle scenario.



(d) Latest prediction scenario.

Figure 5: Comparison of the distribution of the relative error for the two cases for the c_D for each solar and geomagnetic activity scenario.

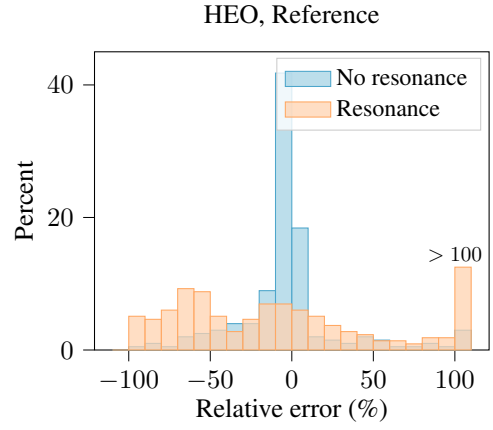


Figure 6: Comparison of the distribution of the relative error for the resonant and non-resonant cases using the estimated c_D and the reference solar and geomagnetic activity scenario.

thin tails resulting on a standard deviation below 50% for all scenarios.

3. IMPACT OF THE BALLISTIC COEFFICIENT

The goal of this section is to investigate a methodology to estimate the ballistic coefficient B of a rocket body and how orbital lifetime predictions can be improved using this estimation. These results were presented at [13] and are included as a summary for their contribution to the overall picture. The tool used for the estimation of B is RACER, which was provided by the European Space Agency. RACER uses Particle Swarm Optimization (PSO) to estimate the B of a body based on real orbital data in the form of TLEs. In real-time operations, it is common to use previous TLEs (or more precise ephemeris data) to estimate the ballistic coefficient of a spacecraft, in order to be used for the orbit propagation required for the operations. In this analysis, however, the goal is to analyze the ballistic coefficient estimated for objects of the same family of stages, thus stages that are expected to be similar, and investigate whether the information obtained from other stages can improve orbital lifetime predictions of other stages from the same family.

3.1. RACER

There are five parameters that can be estimated with RACER: the drag coefficient c_D , the drag cross-sectional area A_D , the mass of the object m , the reflectivity coefficient c_R and the cross-sectional area exposed to the solar radiation pressure A_R . All these parameters can be chosen to be fixed to a specific value or to be estimated by the PSO, setting an upper and lower limit for each of them. For this results, the c_R was fixed to a default of 1.3 for all the objects and the A_R was fixed to the aver-

age cross-sectional area registered in DISCOS for each object. To analyze the results, the resulting c_D , A_D and m were always combined into the ballistic coefficient B .

RACER takes a set of TLEs to be analyzed. Different particles are generated at the epoch of the first TLE available, each one using a different value of the parameters to be estimated. These particles are propagated until the end of the analyzed time period, and their performance is evaluated in terms of the Root Mean Square error (RMS) and of a score depending on the global RMS of the trajectory, and the RMS of the semimajor axis and of the perigee altitude. The particle with the best score is then chosen and perturbed again to generate a new set of particles. The process is repeated until a solution is found which scores below previously established thresholds. RACER, as OSCAR, uses the semianalytical propagator FOCUS.

A moving time window is implemented in RACER to select the TLEs that are analyzed at each time. The width of the time window can also be chosen, and it was set to 1 month for the simulations in this study.

3.2. ORION 38: ballistic coefficient estimation

The stage family chosen for the analysis was ORION 38. Within this dataset, this stage was used as upper stage of both Pegasus XL and Minotaur I launch vehicles. Moreover, it has also been part of the Taurus, Taurus XL, Taurus Lite, Minotaur-C, and Minotaur IV launch vehicles [6]. It is a small stage, with a dry mass of 216 kg, a diameter of 0.97 m and a length of 1.76 m [9, 3]. From these dimensions, the c_D can be calculated using equation (1), resulting in $c_D = 2.0$, and the minimum, average and maximum area can be calculated using the tool CROC (CROSS-section of Complex bodies) of the DRAMA software tool-suite, which results in $A_{min} = 0.73 \text{ m}^2$, $A_{avg} = 1.70 \text{ m}^2$ and $A_{max} = 1.86 \text{ m}^2$. Three different ballistic coefficients can be calculated from these three cross-sectional areas, which in this paper are named B_{min} , B_{avg} and B_{max} in relation to the cross-sectional area that they correspond to. Thus, B_{min} does not correspond to the minimum value of the ballistic coefficient, but to the ballistic coefficient calculated using the minimum cross-sectional area A_{min} .

Figure 7 shows the results obtained for each ORION 38 stage in a different color (the legend shows the satno of each object), with each dot representing the result for a one-month window. The theoretical ballistic coefficients, calculated with the minimum, average and maximum cross sections, are shown as horizontal dotted black lines. The results contained a few outliers, which were removed to improve the readability and quality of the results. The outliers were defined as an estimated ballistic coefficient that deviated by more than three standard deviations from the average value of the ballistic coefficient of an object. A total of 12 outliers were removed out of 668 data points.

It can be observed that there are two objects, with satno

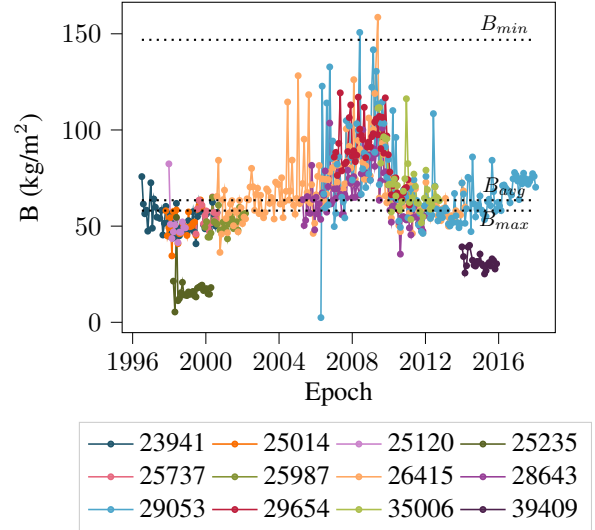


Figure 7: Estimated ballistic coefficient with RACER for the ORION 38 objects. The horizontal dotted lines represent the theoretical ballistic coefficients for reference.

25235 and 39409, that have a very different ballistic coefficient from the others. It can be assumed that both objects had a different stage configuration than the others. The other objects all seem to have ballistic coefficients which stay close to the theoretical B_{max} and B_{avg} most of the time. However, there is a peak after 2008, where the estimated B approaches more the value of the B_{min} .

Figure 8 shows the same results as in figure 7, but the outlier objects have been removed and the ballistic coefficient of each object has been smoothed by taking the centered 5-months rolling average in each epoch. Furthermore, the observed solar activity for the analyzed epochs was plotted as a dotted blue line. The results show a strong correlation between the estimated ballistic coefficient and the solar activity, obtaining higher ballistic coefficient for low solar activity periods. Indeed, the aforementioned peak is now much clearer, and it can be related to the solar minimum around 2009.

While the ballistic coefficient does not depend on the solar activity, what RACER is really estimating is how strong the effect of drag was in order to lead to a certain evolution of the orbital parameters. Atmospheric drag is also proportional to the atmospheric density, which is very challenging to model and depends on the solar and geomagnetic activity. Therefore, even though the ballistic coefficient does not directly depend on the solar activity, the estimated ballistic coefficient is absorbing the error in the modeling of the atmospheric density, which does depend on the solar activity. The ballistic coefficient estimated by RACER is equivalent to:

$$B_{RACER} = B \cdot \frac{\rho_{model}}{\rho_{real}} \quad (2)$$

Where ρ_{model} is the atmospheric density estimated by the

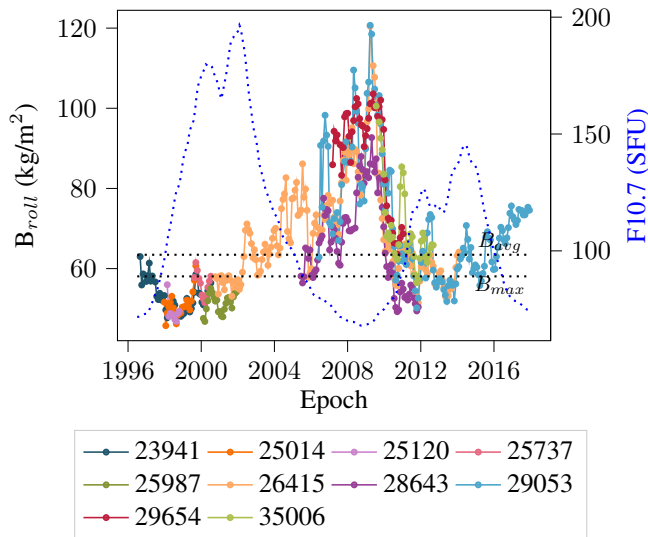


Figure 8: Five-months rolling average of the estimated ballistic coefficient with RACER for the ORION 38 objects. The black horizontal dotted lines represent the theoretical ballistic coefficients for reference. The blue dotted line shows the observed solar activity.

model and ρ_{real} is the real one. The results therefore show that the error of the atmospheric model is not constant for all levels of solar and geomagnetic activity.

3.3. ORION 38: Orbital lifetime estimation

The goal of this section is to analyze if and how the results obtained with RACER can be used to improve the orbital lifetime estimations. In order to assess whether an improvement on the orbital lifetime predictions can be achieved using the results obtained with RACER, a reference prediction without RACER is needed. The chosen reference scenario is using the observed solar and geomagnetic activity values, in order to remove any uncertainties related to inaccurate predictions of these parameters. The propagations were performed with OSCAR using the theoretical $B_{avg} = 63.53 \text{ kg/m}^2$, and the initial orbit corresponding to the first TLE of each object, performing the appropriate transformations with CState.

The evolution of the semimajor axis for the real case plotted from the TLEs (dotted line) and the predicted case (solid line) is shown in figure 9. It can be observed that, even though the predictions seem to work really well for the first four objects, they differ a lot from reality for the others, especially for objects 26415 and 29053. Going back to the results shown in figure 8, these objects are on orbit mostly during a low solar activity period, and their estimated B reaches values that deviate far from the B_{avg} . The average error for this scenario was -1.42 years, and the average relative error was -17%, showing a tendency to underestimate the orbital lifetime.

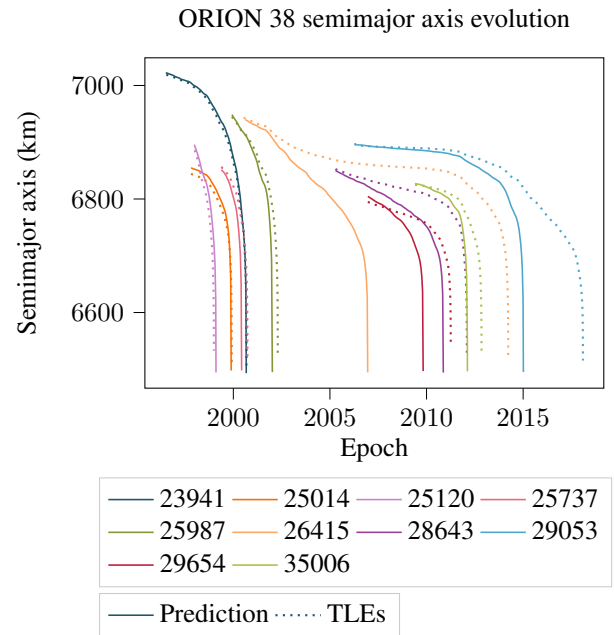


Figure 9: Evolution of the semimajor axis for the analyzed ORION 38 stages using the observed solar and geomagnetic activity and the estimated c_D .

The need for an improvement of the orbital lifetime estimation for these objects is clear. The simplest approach would be to compute the average of all the values obtained for the ballistic coefficient and use this value for the propagations. The data corresponding to the object to be propagated should be excluded from the dataset to compute this average ballistic coefficient, in order to remove any bias introduced by using data from the same object and to make the methodology applicable also when there is still no TLE data from the object.

The resulting average coefficients, after removing the outliers for each object and the outlier objects (25235 and 39409), ranged between 65.62 kg/m^2 and 68.69 kg/m^2 . As OSCAR does not take any value of the ballistic coefficient, but rather the individual quantities (namely mass, drag coefficient and cross-sectional area), the cross-sectional area and mass were kept to the same values used before, and the c_D was modified to match the calculated value for the ballistic coefficient. The obtained results are shown in figure 10.

The tendency with this method was to overestimate the orbital lifetime, with only one object showing a slight underestimation. The general results improved in terms of the absolute error, which was now on average 0.81 years. However, the relative error remained in a very similar magnitude, with an average of 20.87%. This was due to the worsening of the results of the short-lived objects, while the long-lived objects improved.

As the previous results showed a strong correlation of the ballistic coefficient to the solar activity, the second

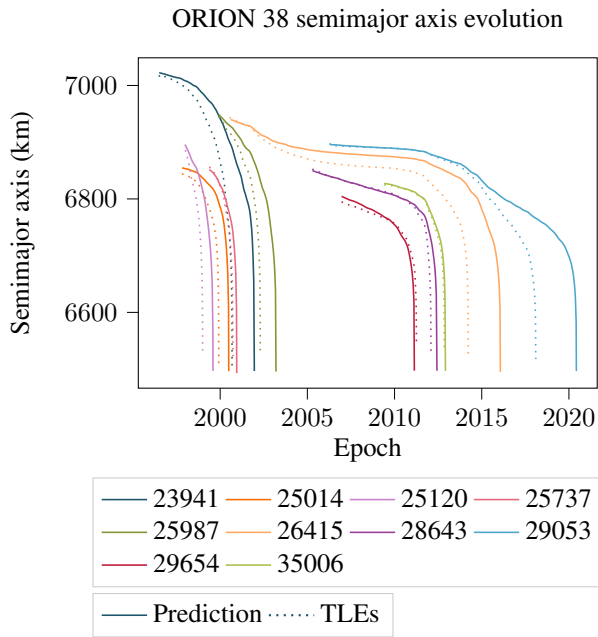


Figure 10: Evolution of the semimajor axis and the perigee altitude for the analyzed ORION 38 stages using the latest prediction scenario and the average ballistic coefficient from RACER.

method that was tested was the use of a "dynamic" ballistic coefficient, which changes value depending on the solar activity level. In order to do this, the propagation was performed in small steps, each with a duration Δt years. In each step, the observed F10.7 is checked and the value of the ballistic coefficient is chosen accordingly.

Only two categories were defined for the solar activity level, high or low, separated by a threshold that was chosen to be at 90 SFU. One ballistic coefficient is calculated for each category, B_{high} and B_{low} , corresponding to the average of the estimated ballistic coefficients during periods of high or low solar activity respectively. Furthermore, the RACER results corresponding to the object to be propagated were removed from the data used to calculate the ballistic coefficients.

The process followed for the orbital lifetime estimation was as follows: a short propagation span Δt is chosen, which here was set to 0.1 years. Once an object is selected, the ballistic coefficients B_{high} and B_{low} corresponding to this object are calculated. This is done by excluding the results corresponding to this object from the dataset of ballistic coefficients estimated by RACER, dividing the data into two categories depending on the solar activity level during the analyzed period, and calculating the average B of each category. It should be noted that the outlier values of B for each object have already been excluded before, as well as the two outlier objects.

When the B_{high} and B_{low} have been calculated, the propagation process is initiated. Starting from an initial orbit

at an initial epoch t_0 , the observed F10.7 at the epoch is checked. If it is above the threshold, the average B for high solar activity B_{high} is chosen. Otherwise, the average B for low solar activity B_{low} is selected. The selected B is then used for the propagation with OSCAR, for a propagation span Δt . The results are then checked to see if a re-entry occurred during the propagation. If it did, the propagation stops and the results are recorded. If a re-entry didn't occur, the orbit at the last propagation epoch becomes the initial orbit for the next propagation. The process is repeated as many times as necessary until a re-entry is found.

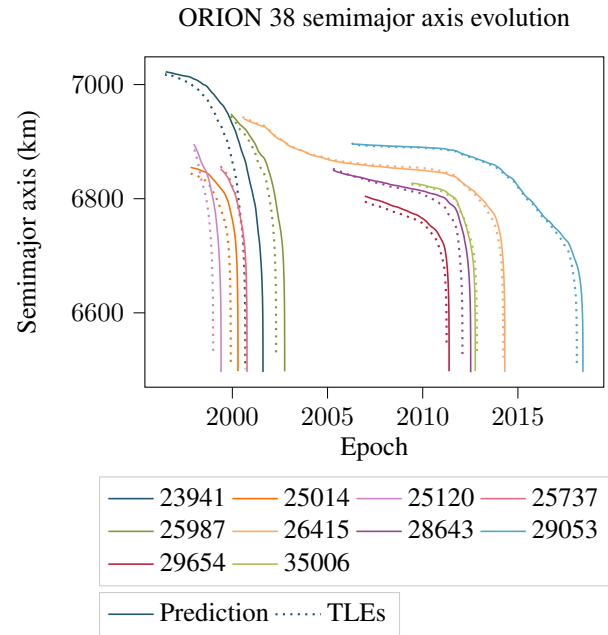


Figure 11: Evolution of the semimajor axis and the perigee altitude for the analyzed ORION 38 stages using the latest prediction scenario and the estimated c_D .

Figure 11 shows the results for the orbital lifetime predictions, compared with the actual TLEs, for the solar activity dependent ballistic coefficient approach explained above. The predictions for objects 23941, 25014, 25120, 25737 and 25987, which had a very small error before, show a worse performance as before, with a tendency to overestimate the orbital lifetime. However, the magnitude of this error still remains small, with a maximum of 0.93 years for object 23941. On the other hand, the predictions of the second half of the objects significantly improved. The case of objects 26415 and 29053 can be highlighted, which initially presented an underestimation of 7.27 and 3.08 years respectively, being the largest errors in the dataset. The predictions with the current approach turned the error into a 0.09 and 0.32 years overestimation respectively. Indeed, all the errors obtained with this approach remain below 1 year. The average error with this approach was 0.31 years, and 11.36% average relative error. This approach therefore significantly improved the results both from the reference and the constant average estimated B methods.

4. CURRENT PMD PRACTICES

The aim of this section is to analyse the current implementation of PMD practices in rocket stages. A previous analysis was performed in [12], which has been updated with more recent data, and the analysis of the CCP has been added. This analysis considers both the current IADC space debris mitigation guidelines and the new policies introduced by the Zero Debris charter. For more details on current PMD practices, ESA's environment report is recommended to the interested reader [11].

The dataset used for this analysis was extracted from ESA's DISCOS database [2], and the TLEs for each object were extracted from spacetrack [4]. The dataset includes 945 rocket stages which were launched into orbits crossing LEO between 2016 and 2023. It includes information about launch and re-entry epochs, initial and destination orbits, mass and dimensions of the stages, as well as the launcher and launcher family that they correspond to. The latest orbits of non-re-entered objects, required for the propagation for this analysis, were extracted from the TLEs of the object.

The study aims to analyze the orbital lifetime and CCP of the objects in the dataset. For the objects which have already re-entered, this implied the computation of their orbital lifetime and CCP based on their TLEs, while objects that have not yet re-entered had to be propagated. OSCAR was used for the propagation, using the latest prediction solar and geomagnetic activity scenario. The propagation span in OSCAR was set to a maximum of 300 years. The available mass and average cross-section were used for the propagation, and the c_D for each object was estimated using equation (1) and the dimensions available for each object. When information on the dimensions of a stage could not be found, a default $c_D = 2.2$ was used. Moreover, the destination orbits of objects that performed PMD were also propagated in order to approximate their behavior if they would not have performed PMD.

4.1. Cumulative Collision Probability

The approach used to calculate the CCP uses the data from the MASTER (Meteoroid And Space debris Terrestrial Environment Reference) model and is based on the spatial density of the orbital shells that the objects pass through.

MASTER provides the spatial density of objects above a specific size for each orbital shell. These orbital shells are spherical shells around Earth delimited by a lower and maximum altitude. During this work, the population of objects larger than 1 cm in diameter was used, as it is the one used in the requirements of the Zero Debris policy.

The collision probability of an object orbiting in a circular orbit contained entirely in a specific orbital shell can

be calculated as:

$$P_c = 1 - \exp(-\rho v A \Delta t) \quad (3)$$

Being ρ the spatial density in the orbital shell, v is the impact velocity, even though the orbital velocity of the object was used in this model for simplicity, A is the cross sectional area of the object and Δt the time interval for which the collision probability is calculated. This formula is derived by assuming a Poisson distribution with $N = \rho v A \Delta t$ being the expected rate of occurrences (collisions). The collision probability is then calculated as the conjugate of the probability of zero collisions, resulting in equation (3).

When an orbit is crossing several orbital shells, however, the calculation becomes a bit more complicated. The first step then would be to calculate crossings of the orbit with the altitude boundaries between shells. Then, the average velocity in each shell and the time spent in each of them can also be calculated. The collision rates of each shell can be added up, which in the end turns into equation (4) for the calculation of the cumulative collision probability due to the contribution of each shell.

$$P_c = 1 - \exp\left(-A \sum_{i=1}^n \rho_i v_i \Delta t_i\right) \quad (4)$$

When the cumulative collision probability has to be computed for the trajectory of a decaying object, the idea is the same: the time spent in each orbital shell is calculated, as well as the average velocity in each shell. Then, the collision rates are added and the cumulative collision probability can be calculated using equation (4).

The trajectories used in this work corresponded, in the case of re-entered objects, to their processed TLEs, and in the case of objects which did not re-enter yet, to the aggregation of their processed TLEs and the propagated trajectory with OSCAR.

This approach was chosen due to its computational speed, which was needed to process a large dataset. It comes, however, with two major limitations that should be discussed. Firstly, it takes into account only the average spatial density on each orbital shell, but reality is more complex. The biggest impact of this assumption corresponds to the lack of consideration of the inclination of the orbit, which strongly influences the distribution of the space debris population. The collision probability will therefore be underestimated for inclinations that tend to be especially crowded, such as Sun-synchronous inclinations. Secondly, the use of the orbital velocity instead of the impact velocity will lead to a general underestimation of the orbital lifetime, as the mean impact velocity in LEO is around 10 km/s.

4.2. Processing of the TLEs

In order to make sure that errors on the TLEs did not introduce mistakes which could significantly affect the results, they had to be processed. It is first important to note that, for our application which is the computation of the CCP, deviations that are not lasting on time, or small deviations on the semimajor axis, would not have a great impact on the calculated CCP. A real impact would come from long-sustained significant deviation of the semimajor axis or eccentricity.

The steps used for the processing of the TLEs were:

1. Corrected TLEs were discarded. Sometimes, a second TLE is published shortly after the publication of another one which intends to correct the first one. Therefore, when two TLEs are spaced in less than half an orbital period, the first one was discarded [20].
2. A simple filter was set up to discard single aberrant TLEs when a sudden significant increase of the semimajor axis was detected. This was based on the fact that all the analyzed objects are decommissioned rocket stages which are not expected to manoeuvre.
3. A sliding backwards window was used to filter the first TLEs, as they are known to be prone to mistakes. This sliding window was applied on the semimajor axis of the TLEs, using a linear regression of the TLEs within the window to estimate the expected value of the semimajor axis of the next TLE. The deviation of the next TLE from the predicted value is then evaluated with preset tolerances to decide whether it is an outlier. This was based on the described filter in [20].
4. Similarly, a forward sliding window was used to analyse the last TLEs of the objects which needed to be propagated, thus those which did not re-enter yet, in order to make sure that the propagation was not started from a faulty TLE.
5. When there were big gaps of time with no TLEs, these were filled with a linear approximation between the two TLEs on the edges of the empty interval. While the orbital evolution is obviously not linear, this was found to be enough to complete such periods for the current application.

4.3. Results orbital lifetime

We will first look at the results obtained regarding the orbital lifetime of the stages. The results are divided by launcher family. The analysis shows only the launcher families which performed more than 5 launches during the studied period. Figure 12 shows the proportion of objects from each launcher family which fall within a specific lifetime interval, with those intervals being defined

in years. Thus, the dark green bars represent the proportion of objects of each family with lifetimes between 0 and 1 year, the light green between 1 year and 5 years, and so on. This figure allows to assess the level of compliance of each family with the 25-years guideline, as well as with the new 5-years standard of the Zero Debris policy.

The positive note comes from families such as Antares 200, Atlas V, Ceres-1, or Delta IV, whose stages all re-enter in less than 5 years. Moreover, Epsilon, Kuaizhou, Long March 7, and Vega complied with the 25-years rule for all their stages. On the other hand, the lowest compliance rates come from the Ariane 5 and the Rokot families. Both rockets were designed before the IADC guidelines were established, and they were therefore not designed to perform a PMD. The Rokot launchers, however, have been performing manoeuvres aimed at reducing their orbital lifetime, but they were far from being sufficient. The Ariane 5 launchers do not have reignition capability, and they tend to launch to Geostationary Transfer Orbits (GTO) which often have long orbital lifetimes. It is intended that the Ariane 6 launcher will solve this problem. While it failed to perform a correct PMD on its maiden flight in July 2024, the disposal was successful on its second flight in March 2025 [1].

It is also worth to note the performance of the Falcon launchers, as they launched far more than any other launcher during this period, with a total of 257 stages registered in this dataset. A total of 209 of these stages performed controlled re-entries, with the objective to also reduce the risk on-ground. However, some of the remaining stages present significantly large orbital lifetimes, with 10 of them showing expected orbital lifetimes above 50 years and 15 not being compliant with the IADC 25-years guideline.

Figure 13 shows the number of objects that were launched by each family, with the dark green bar representing those which performed a controlled re-entry, the light green those which performed an uncontrolled PMD manoeuvre and the red those which did not perform any PMD manoeuvre. Moreover, the average orbital lifetime of the objects launched by each family is represented by a blue solid line, and the purple dashed line represents the orbital lifetime that the stages would have had if they would not have manoeuvred, which was calculated by propagating their destination orbits.

The number of stages is significantly dominated by the Falcon family, which corresponds to over a 25% of the objects in the database. Despite their high percentage of PMD manoeuvres, the 43 non-manoeuvred Falcon stages are still more than most families launched during that period. Their average orbital lifetime remains however low with about 7.5 years, due to the high percentage of objects that re-entered almost immediately after their orbit insertion.

The largest reduction of the orbital lifetime achieved by the PMD manoeuvres corresponds to the Delta IV family,

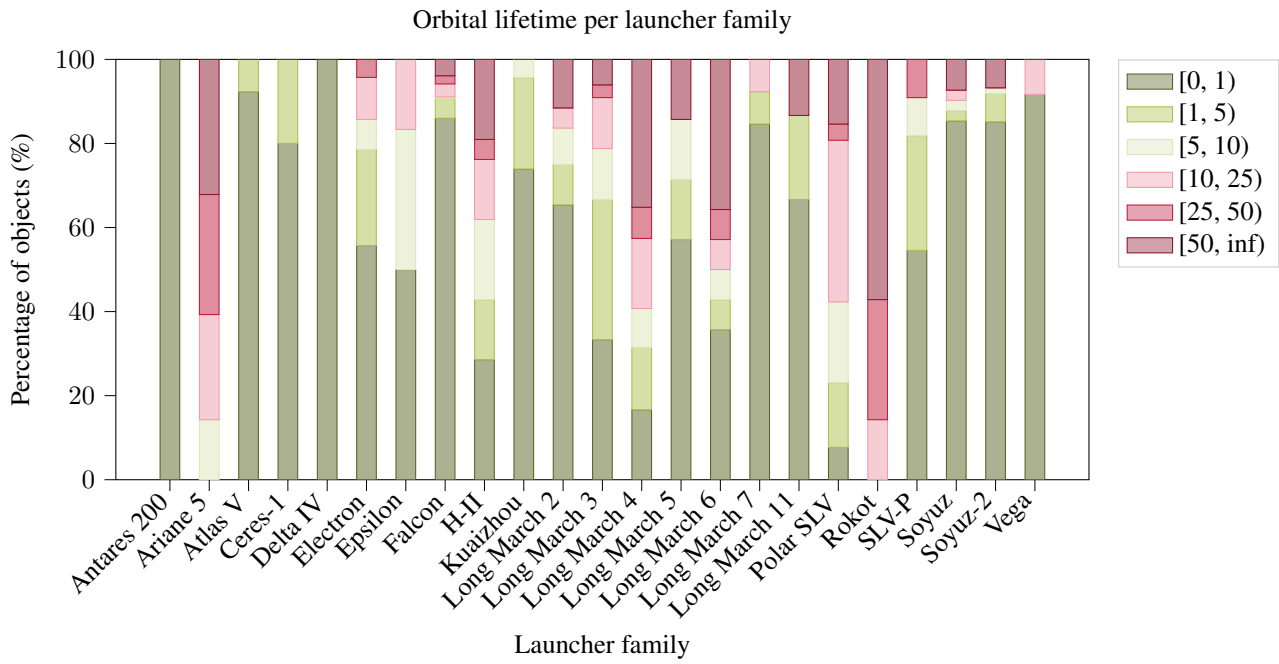


Figure 12: Proportion of objects by each launcher family in a specific lifetime interval, which is defined in years.

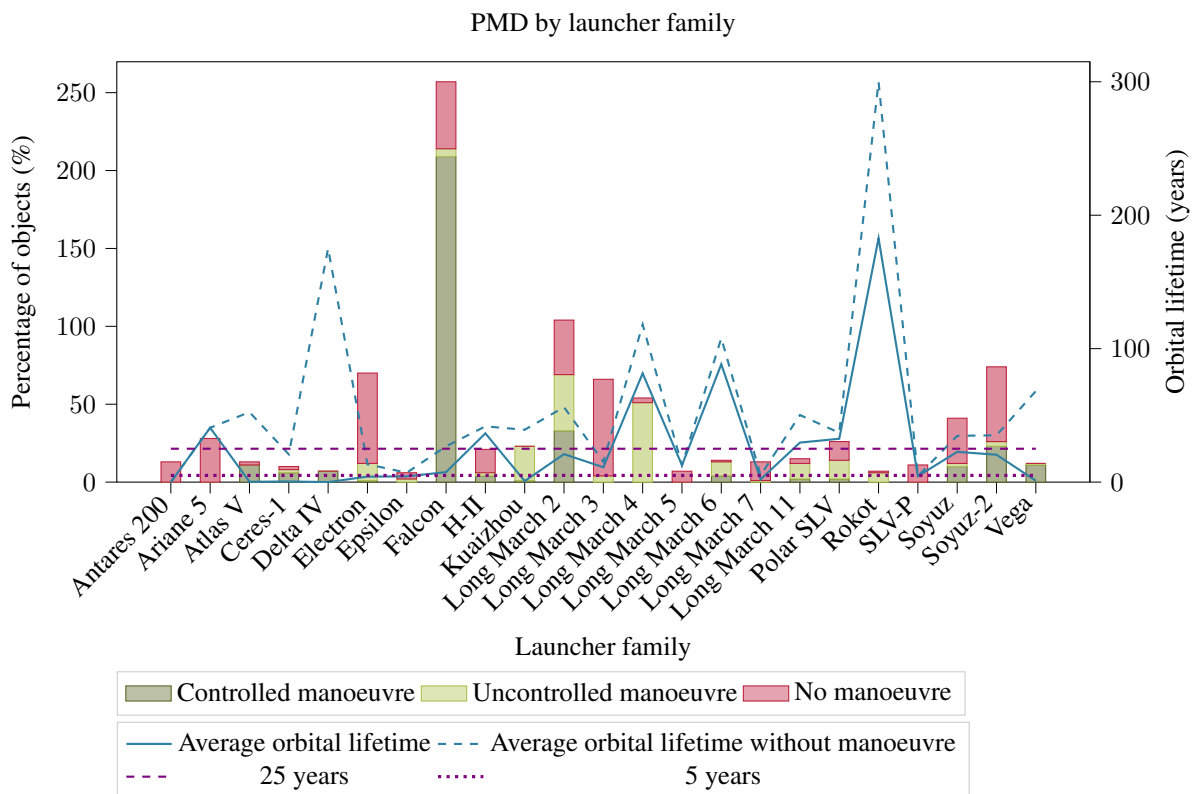


Figure 13: Number of stages per launcher family, divided on those which performed a controlled PMD (dark green bar), an uncontrolled PMD (light green bar) and those which did not perform any PMD (red bar), and average orbital lifetime of the stages of each family, both real (blue solid line) and in the case that no PMD would have been performed (blue dashed line). The horizontal purple lines represent an orbital lifetime of 25 years and 5 years respectively.

whose average orbital lifetime without PMD was around 175 years, which got reduced to virtually no orbital lifetime, as all Delta IV stages performed a controlled re-entry. On the other hand, the Ariane 5, H-II, Long March 4, Long March 6, Long March 11, Polar SLV and Rokot families all had average orbital lifetimes above the 25-years limit. With Rokot being the clear outlier with over 180 years of average orbital lifetime, the Long March 4 and 6 families can also be highlighted, both with average orbital lifetimes above 80 years. The comparison with the average lifetime without manoeuvre, however, shows the effectiveness of the measures taken to reduce the orbital lifetime, as only 8 out of the 23 studied families would have had average lifetimes below 25 years without any PMD. It can be noted that the average lifetime of the Rokot launchers is underestimated due to the 300 years limit on the propagation span, as several Rokot stages reach this limit even after PMD. In the scenario without PMD, propagating the destination orbits, all Rokot stages reach the 300 years propagation span limit.

In view of the newly established requirements by the Zero Debris policy, however, it is important to note that only 10 out of the 23 families analyzed here had an average orbital lifetime below 5 years. These were Antares 200, Atlas V, Ceres-1, Delta IV, Electron, Epsilon, Kuaizhou, Long March 7, SLV-P and Vega.

4.4. Results Cumulative Collision Probability

This section will take a look at the cumulative collision probability (CCP) of the stages until their re-entry with respect to the 1 cm population. The process followed to estimate the CCP was explained in section 4.1. The decision to perform this analysis with respect to the 1cm size population was based on the new Zero Debris standard, which sets a requirement of a CCP below 1 in 1000 with respect to this size population. The CCP with respect to the 1 cm population will be expressed from now on as CCP(1cm).

Figure 14 shows the proportion of objects of each launcher family within each CCP interval. Therefore, the darkest green represents the objects with CCP(1cm) below 10^{-6} , the medium green the objects with CCP(1cm) between 10^{-6} and 10^{-5} , and so on.

It can be seen than no Rokot stage would have been compliant with the Zero Debris requirements, with over half of the Rokot stages presenting a probability of collision above a 10%. Moreover, the CCP(1cm) of the Rokot stages is likely to be strongly underestimated, as the propagation was stopped after 300 years when many of these stages were still located in very high orbits which are also less crowded. These stages would in reality keep accumulating CCP for a long time, before finally making their way to lower and more crowded orbits which would also have a strong contribution to the CCP. Additionally, the Falcon, Long March 2, Long March 4, Long March 6, Long March 11 and Polar SLV families all had stages with CCP(1cm) over a 10%.

It can also be noted that only one stage out of the 28 Ariane 5 stages in the dataset had a CCP(1cm) below 0.001, thus compliant with the Zero Debris policy. The families Antares 200, Atlas V, Ceres-1, Delta IV, Epsilon had all the stages with CCP(1cm) below 0.001. It can be noted that these are almost the same families whose stages would have also been compliant with a 5-years orbital lifetime, only with the addition of the Epsilon family.

Figure 15 shows again the number of objects launched by each launcher family and whether they manoeuvred or not. The solid blue line represents the addition of the CCP(1cm) of all the objects of each launcher family. Thus, it would represent the expected number of collisions with respect to the 1cm population of all the stages of each family.

There are 4 families whose cumulative CCP(1cm) is above one, thus it would be expected that at least one collision would take place for a stage belonging to that family. These families are Long March 2, Long March 4, Long March 6 and Rokot. The most predominant peaks are clearly those of Long March 2, Long March 4 and Long March 6 families. The biggest reduction of the CCP(1cm) was achieved by Falcon, thanks to the controlled re-entry of over 200 stages.

The pie chart in figure 16 represents the proportion of the total risk introduced to the environment by all the rocket stages launched in the studied period that correspond to each rocket family. Thus, from the sum of the CCP(1cm) of all the stages in this study, which percentage corresponds to each launcher family.

The Long March 2 and Long March 4 families took each over 30% of the total CCP(1cm) during the studied period, and the Long March 6 over a 15%. These are by far the launcher families which contributed the most to the total risk during the studied period. Indeed, all the Long March stages together represented over a 70% of the total risk introduced by rocket stages during this period in terms of CCP(1cm). It can be noted that the Long March 2 family was originally showing reasonable results on the orbital lifetime of their stages, with an average below 25 years and almost 90% compliance with the 25-years rule. However, most of these stages are located in orbits with apogee altitudes around 800 km, which corresponds to very crowded orbital altitudes, in addition to being rather big stages, which resulted in the massive 30.1% of the total risk. This effect could be even stronger with an approach that would consider the inclination for the calculation of the CCP, as these stages are also located in Sun-synchronous inclinations, which are also the most crowded around that altitude.

5. CONCLUSION

The paper has presented the results obtained during the project ASCenSIon in the topic of PMD of rocket bodies.

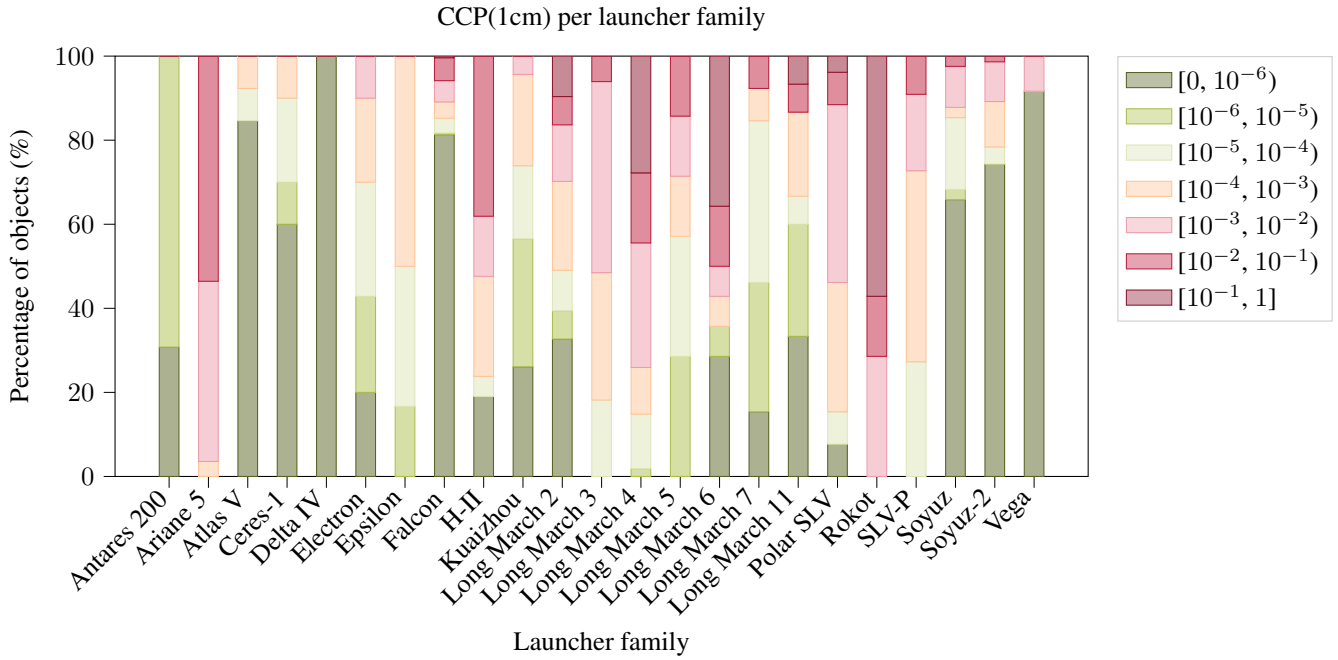


Figure 14: Proportion of objects by each launcher family in a specific CCP(1cm) interval.

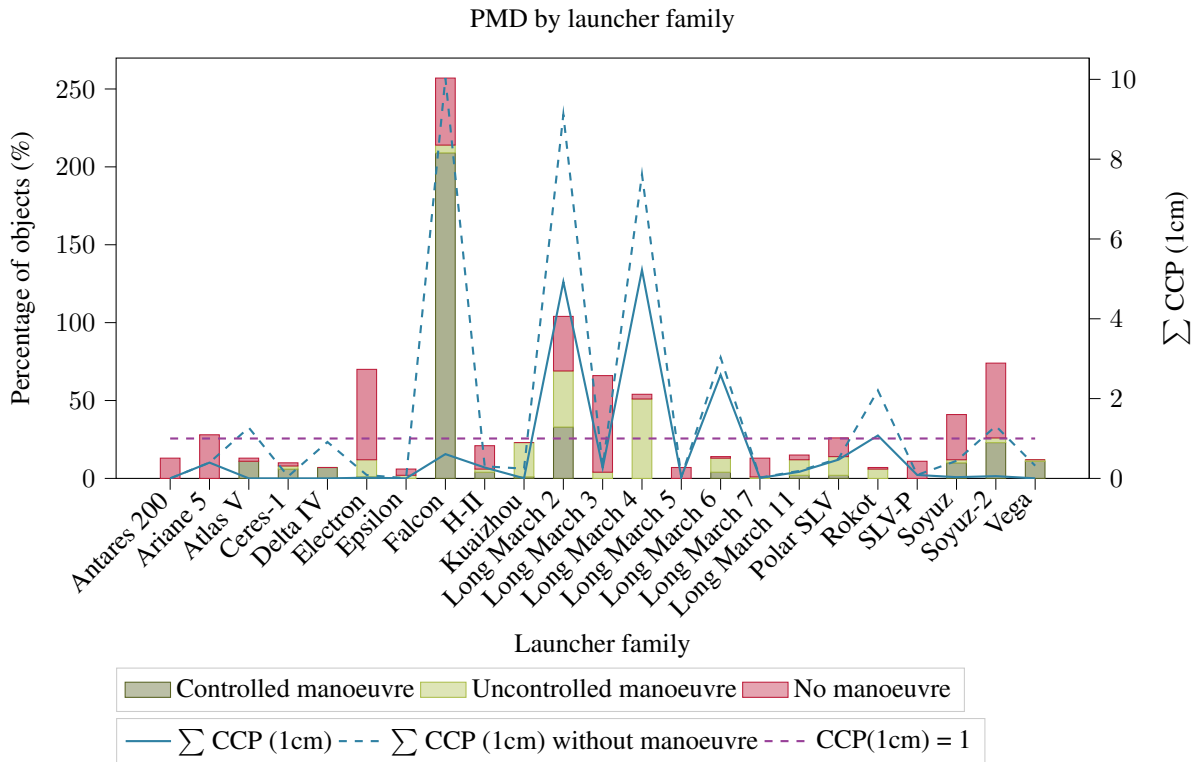


Figure 15: Number of stages per launcher family, divided on those which performed a controlled PMD (dark green bar), an uncontrolled PMD (light green bar) and those which did not perform any PMD (red bar), and the sum of the CCP(1cm) of all the stages of each family, both real (blue solid line) and in the case that no PMD would have been performed.

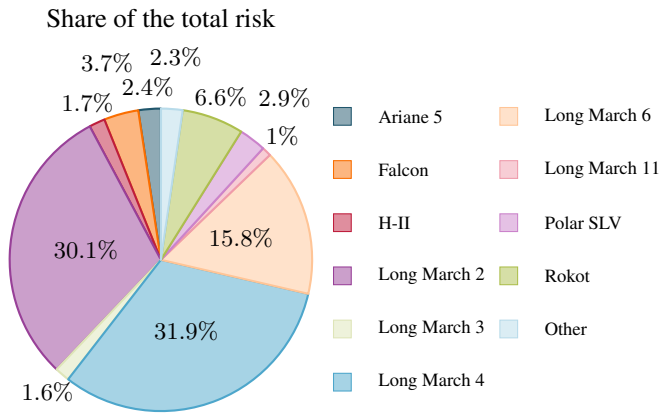


Figure 16: Pie chart showing the proportion of the total CCP(1cm) corresponding to each launcher family.

The first analysis presented studied the accuracy of current methodologies for the estimation of the orbital lifetime, for LEO and HEO objects. Even using the observed solar and geomagnetic activity, the distribution of the error showed a standard deviation of around 30%, inviting to think that currently used margins as the 5% recommended by ISO [5] might not be enough. Moreover, the use of a specific c_D for each rocket body, based on their dimensions and approximating their shape as cylinder, proved to be a better approximation than the default $c_D = 2.2$. Many parameters were shown to affect the accuracy of the prediction in LEO, such as the launch year, the time in orbit or the ballistic coefficient of the object.

The HEO predictions were shown to be a great challenge. The distribution of the error obtained showed standard deviations of over 100% in all scenarios, which leaves very little confidence on the results of the estimations. The results did not deviate much between solar and geomagnetic activity scenarios, nor with the use of different drag coefficients. However, separating the objects between those reaching the Sun-synchronous resonance and those which do not reach it, led to completely different results, suggesting that conventional methods for orbital lifetime estimation can be applicable for HEO objects if they do not go through this resonance while statistical methods are definitely required for HEO objects which pass through the resonance.

The tool RACER was used to estimate the ballistic coefficient of objects belonging to the ORION 38 family. The results showed a correlation between the estimated ballistic coefficient and the solar cycle, which can be explained through the errors induced by the solar activity on the atmospheric model. It was shown that using a ballistic coefficient that changes depending on the solar activity level can help to correct for this error and improve orbital lifetime predictions. However, further analysis is required to assess whether this methodology can be applied to other stages.

Finally, current PMD practices were analysed for differ-

ent launcher families in terms of their orbital lifetime and CCP(1cm). While most families performed well with respect to the 25-years lifetime, an additional effort will be required to reduce this limit to 5 years. Moreover, the stages that performed the worst in terms of orbital lifetime were not necessarily the worst in terms of CCP(1cm), as this is also dependent on the orbit and the cross-section of the object. Three single families, Long March 2, Long March 4, and Long March 11, took together over 75% of the total risk introduced on orbit by rocket stages launched during the studied period.

ACKNOWLEDGMENTS

The project leading to this application has received funding from the European Union's Horizon 2020 research and innovation programme under the Marie Skłodowska-Curie grant agreement No 860956.

REFERENCES

1. Ariane 6 takes flight for the second time. https://www.esa.int/Enabling_Support/Space_Transportation/Ariane/Ariane_6_takes_flight_for_the_second_time#:~:text=Europe's%20newest%20rocket%2C%20Ariane%206,CSO%2D3%20satellite%20to%20orbit., visited on 21/03/2025.
2. DISCOS web. <https://discosweb.esoc.esa.int/>, visited on 08/04/2024.
3. Norbert Brügge, table of contents. <https://www.b14643.de/>, visited on 08/04/2024.
4. space-track.org. <https://www.space-track.org>, visited on 18/02/2022.
5. International Standard ISO 27852:2016, Space systems - estimation of orbit lifetime. Technical report, ISO, July 2016.
6. Orion motor series. Technical report, Northrop Grumman, 2016.
7. International standard ISO 24113, space systems - space debris mitigation requirements. Technical report, ISO, July 2019.
8. IADC space debris mitigation guidelines. Technical report, Inter-Agency Space Debris Coordination Committee, Mar. 2020.
9. Pegasus payload user's guide. Technical report, Northrop Grumman, 2020.
10. ESA space debris mitigation requirements, ESSB-ST-U-007 issue 1. Technical report, ESA, Oct. 2023.
11. ESA's annual space environment report. Technical report, ESA Space Debris Office, 2024. https://www.esa.int/Space_Safety/Space_Debris/ESA_Space_Environment_Report_2024, visited on 21/03/2025.

12. L. Ayala Fernández, C. Wiedemann, and V. Braun. Analysis of space launch vehicle failures and post-mission disposal statistics. *Aerotecnica Missili & Spazio*, 101(3):243–256, 2022.
13. L. Ayala Fernández, C. Wiedemann, V. Braun, and S. Lemmens. Impact of the ballistic coefficient estimation on orbital lifetime predictions of rocket bodies. In *74th International Astronautical Congress (IAC)*, 2023.
14. L. Ayala Fernández, C. Wiedemann, V. Braun, and S. Lemmens. Uncertainty in remaining orbital lifetime estimation after post-mission disposal. In *24th Advanced Maui Optical and Space Surveillance Technologies Conference (AMOS)*, 2023.
15. V. Braun, S. Lemmens, B. Reihls, H. Krag, and A. Horstmann. Analysis of breakup events. In *7th European Conference on Space Debris*, Apr. 2017.
16. V. Braun, N. Sánchez-Ortiz, J. Gelhaus, C. Kerschull, S. Flegel, M. Möckel, C. Wiedemann, H. Krag, and P. Vörsmann. Upgrade of the esa drama oscar tool: Analysis of disposal strategies considering current standards for future solar and geomagnetic activity. *Proceedings 6th European Conference on Space Debris*, 2013.
17. ESA Space Debris Mitigation WG. ESA space debris mitigation compliance verification guidelines, ESSB-HB-U-002. Technical report, European Space Agency, Feb. 2023.
18. R. D. Klett. Drag coefficients and heating ratios for right circular cylinders in free-molecular and continuum flow from mach 10 to 30. Technical report, Sandia Corporation, Aerospace Nuclear Safety Research Report, 1964.
19. C. Le Fèvre, H. Fraysse, V. Morand, A. Lamy, C. Cazaux, P. Mercier, C. Dental, F. Deleffie, and D. Handschuh. Compliance of disposal orbits with the french space operations act: The good practices and the stela tool. *Acta Astronautica*, 94(1):234–245, 2014.
20. M. Rasotto, G. D. Mauro, D. G. A. Lidtke, and R. Laugier. Technology for improving re-entry predictions of european upper stages through dedicated observations (ESA ITT AO/1 8155/15/D/SR). Technical report, Dinamica, University of Southampton, CNRS, 2016.
21. D. K. Skoulidou, A. J. Rosengren, K. Tsiganis, and G. Voyatzis. Dynamical lifetime survey of geostationary transfer orbits. *Celestial Mechanics and Dynamical Astronomy*, 130(77), 2018.